Contrasting Kinetics of Highly Similar Chloroalkane Reductive Dehalogenases

Katherine Picott[a] and Elizabeth A. Edwards[a,b]#

[a]Department of Chemical Engineering and Applied Chemistry, University of Toronto, Toronto, Ontario, Canada

[b]Department of Cell and Systems Biology, University of Toronto, Toronto, Ontario, Canada

Running Head: Chloroalkane RDase Kinetic Comparison

#Address correspondence to Elizabeth A. Edwards, elizabeth.edwards@utoronto.ca.

Abstract

Chloroform and trichloroethanes are pervasive groundwater contaminants for which bioremediation has been an effective treatment strategy. Reductive dehalogenase (RDase) enzymes from organohalide-respiring bacteria are essential for their remediation under anaerobic conditions. RDases are responsible for dehalogenating these chlorinated solvents, leading to their removal. This work explores the kinetic characteristics of three closely related *Dehalobacter* chloroalkane-reductases—TmrA, CfrA, and AcdA—and identifies differences between their activity on chloroform (CF), 1,1,1-trichloroethane (TCA), and 1,1,2-TCA. The side-by-side comparison of these enzymes has emphasized that TmrA and AcdA are specialized toward CF with both having 4-fold higher maximum specific activity (V_{max}) on CF than 1,1,1-TCA, whereas, CfrA has very similar rates on both CF and 1,1,1-TCA. AcdA is the most sensitive to substrate inhibition by CF and 1,1,2-TCA, and inhibition by a common co-contaminant trichloroethene. Finally, the reduction of 1,1,2-TCA, which can produce both 1,2-dichloroethane and vinyl chloride, was assessed for each enzyme. Interestingly, each enzyme has a distinct preference for the major product it produces, indicating a favoured reaction pathway. Despite over 95% sequence identity, TmrA, CfrA, and AcdA exhibit substantial differences in kinetic behaviour, highlighting the importance of understanding such nuances for informed bioremediation strategies.

Keywords

Dehalobacter, chloroform, trichloroethane, enzyme kinetics, reaction rate, bioremediation, dechlorination

Synopsis

Three similar dechlorinating enzymes were found to have distinct reaction rates and levels of sensitivity to inhibition. These differences have implications for the enzymes' use in bioremediation.

Introduction

Chloroform (CF) and isomers of trichloroethane (TCA) are widespread groundwater contaminants and are included on the Substance Priority List by the United States' Agency for Toxic Substances and Disease Registry and Environmental Protection Agency [1]. CF, 1,1,1-TCA, and 1,1,2-TCA were commonly used industrially as solvents, degreasers, and reactants [2–4]. Bioaugmentation is a convenient and economical method of remediating sites contaminated with these compounds. There are several commercialized bioaugmentation cultures that target CF, 1,1,1-TCA, and 1,1,2-TCA. These include ACT-3 and KB-1 Plus CF® supplied by SiREM (Guelph, Canada) and AusCF supplied by Novorem (Moss Vale, Australia).

These bioaugmentation cultures are all mixed communities that contain *Dehalobacter*, an obligate organohalide-respiring bacteria (OHRB) [5–8]. All OHRB require reductive dehalogenases (RDases) as the terminal enzyme in their electron transport chain [9]. RDases catalyze the reduction of specific organohalide compounds—specificity depends on the enzyme itself—and in doing so, they remove one halogen through a hydrogenolysis pathway or two halogens through a dihaloelimination pathway [9]. All RDases require a cobamide and two [4Fe-4S] clusters as cofactors [9], but beyond the similar cofactors the diverse RDase family has conserved structural motifs. For example, the two structurally characterized RDases—PceA and NpRdhA—have less than 20% protein sequence identity but highly conserved protein fold features [10,11]. RDases with high protein sequence identity (>90%) are classified into ortholog groups (OGs), which help predict putative substrates based on homology to characterized RDases [12,13].

This report focuses on three enzymes from OG 97; an OG containing RDases that dechlorinate CF and TCAs. TmrA, CfrA, and AcdA have all been identified from *Dehalobacter* sp. that are active in the aforementioned bioaugmentation cultures—TmrA from *Dehalobacter* sp. UNSWDHB in CFH2 (commercialized as AusCF) [14,15], CfrA from *Dehalobacter* sp. CF in ACT-3 [16], and AcdA from a *Dehalobacter* sp. in the enrichment SC05-UT (the latter two commercialized as formulations of KB-1 Plus CF®) [8,17]. These enzymes are over 95% identical to each other on the amino acid level yet display varying levels of activity on the same substrates and have widely different fractionation patterns in stable isotope analysis suggesting that their mechanisms of action may be distinct [18,19]. Relative substrate selectivity has been compared in whole cells, cell-free extracts, and some partially purified enzymes [14,16,17,20], but not in a side-by-side comparison of the

enzyme's kinetic activity. The recent ability to heterologously express these enzymes in a common host enables a true direct comparison. More in-depth knowledge of how different RDases interact with the same substrate can better inform bioaugmentation strategies and sequence-substrate-activity relationships provide insight into the mechanisms of the enzyme family. Here, we analyze the kinetics of heterologously produced TmrA, CfrA, and AcdA against three substrates: CF, 1,1,1-TCA, and 1,1,2-TCA. We also assess the relative inhibition of each enzyme by a common co-contaminant, trichloroethene (TCE), and look at structural features that could contribute to the observed differences.

Materials and Methods

Materials

All chemicals, unless otherwise stated, BugBuster®, and filter tubes were purchased from MilliporeSigma (Burlington, MA, USA). All growth media, antibiotics, and induction agents were purchased from BioShop Canada Inc. (Burlington, ON, Canada). Bradford reagent was purchased from Bio-Rad Laboratories Ltd. (Hercules, CA, USA). All glass syringes were purchased from Hamilton Company (Reno, NV, USA). Steal washers were purchased from Amazon.com Inc. (Seattle, WA, USA). All gasses were supplied from Linde Canada Inc. (Mississauga, ON, Canada). A Coy vinyl anaerobic chamber was used to maintain an anaerobic atmosphere (Coy Laboratory Products Inc., Grass Lake, MI, USA); this is referred to as a glovebox throughout. Gas chromatography materials were purchased from Agilent Technologies (Santa Clara, CA, USA).

Enzyme Expression

Three RDases from *Dehalobacter* were heterologously expressed in *Escherichia coli*: TmrA (accession: WP_034377773) from *Dehalobacter* sp. UNSWDHB [14], CfrA (AFV05253) from *Dehalobacter* sp. CF [16], and AcdA from a *Dehalobacter* in the SC05 bioaugmentation culture (XCH81453) [17]. The construction of the expression plasmids *p15TVL-tmrA*, *p15TVL-cfrA*, and *p15TVL-acdA* and the production of their expression strains have been described elsewhere [17,20]. Each expression plasmid was expressed in *E. coli* BL21(DE3) *cat-araC*-P_{BAD}-*suf*, *ΔiscR::kan, ΔhimA::*Tet^R with co-expression of the *pBAD42-BtuCEDFB* plasmid [21,22]. The *pBAD42-BtuCEDFB* plasmid was generously provided by the Booker Lab (Pennsylvania State University,

PA, USA). *E. coli* BL21(DE3) *cat-araC*-P_{BAD}-*suf*, *ΔiscR::kan, ΔhimA::*Tet^R, was generously provided by the Antony and Kiley Labs (St. Louis University School of Medicine, MO, USA; University of Wisconsin-Madison, WI, USA). The expression and nickel-affinity chromatography purification protocols followed those published elsewhere [17,20]. Minor modifications to the protocol are the use of Luria Broth (LB) media and the removal of Triton X-100 and glycerol from the wash, elution, and storage buffers. All plasmids are in Tables S1 and a detailed methodology can be found in Supplemental Text S1.

The protein concentration was measured by Bradford assay [23], and the purity was estimated by sodium dodecylsulfate polyacrylamide gel electrophoresis (SDS-PAGE) using Image Lab 6.1 software (2022, Bio-Rad Laboratories, Inc.), (SDS-PAGE in Figure S1). The protein was stored in liquid N_2, freeze-thaw stability had been confirmed in previous experiments, and fresh enzyme from the same batch was used for each experiment. The standard deviation of triplicate protein concentration measurements was incorporated into the enzyme activity error (concentrations used in Table S2).

Kinetic Experimental Method Design and Assumptions

The kinetic assays were performed in the barrel of a 1-mL glass gas-tight Hamilton syringe because the substrates and products are volatile and partition differentially into the headspace. During preliminary tests, we observed a poor mass balance between substrates and products when assays were performed in a vial with a headspace since the assumption of equilibrium between the liquid and gas phase was not valid on such a short time scale. Therefore, we sought a method without headspace but where the volume could change. Further, the use of a 1-mL syringe reduced the amount of enzyme required for each assay and allowed for more accurate timepoint sampling. By using a syringe as the reaction vessel, we can more safely assume that no substrate or product is lost; thus, the initial amount of substrate was calculated from the amount of product and remaining substrate.

The elimination of the headspace, in turn, caused difficulty in mixing the reaction, as seen in preliminary tests that resulted in inconsistent rates (data not shown). Thus, we used a small 3.2 mm stainless steel washer inside the barrel of the syringe as a physical mixer to prevent the reaction from being diffusion-controlled. Using the washer, we assume that these reactions are well-mixed and that the rates are governed by the rate-limiting step in substrate catalysis.

Detailed descriptions of the assay setup, data analysis, and kinetic model assessment are provided in Supplemental Texts S2-4.

Kinetic Assay – Vial Set-up

All kinetic assays were performed in an anaerobic glovebox filled with a gas mix containing 10% CO_2/10% H_2/Bal. N_2 (v/v). All materials were equilibrated in the glovebox atmosphere for at least 48 hr before use. A series of vials were used to prepare the reaction buffer for 15 different concentrations of the substrate to produce a full Michaelis-Menten curve. The reactions themselves took place in glass syringes—the prepared buffer was taken from the vial and the desired enzyme was added to the syringe afterward to keep the stock buffer clean. Four reactions total were done using the same stock buffer vial (enzyme-free negative control, TmrA, CfrA, and AcdA).

The assay buffer and substrate mixtures were prepared in sixteen 11-mL vials with mininert caps. Each vial was prepared so that the final liquid volume would be 6 mL with 5 mL headspace. Reaction buffer containing 50 mM Tris-HCl (pH 7.5) and 1 mM methyl viologen (MV) was added to each of the vials—volume varied depending on the predestined substrate concentration. The vials were capped, and the substrate was delivered to the desired concentration from either a saturated water stock or the neat substrate using a gas-tight glass syringe (Tabls S3). Each kinetic assay was performed as a set of at least 15 varying substrate concentrations with one substrate-free vial. The target aqueous substrate concentration ranges for each substrate were 10 μM–1.5 mM chloroform (CF), 5 μM–2 mM 1,1,1-trichloroethane (TCA), and 10 μM–5 mM 1,1,2-TCA. However, the actual initial substrate concentration was calculated by summing the remaining substrate and the product measured by gas chromatography-flame ionization detection (GC-FID). All vials (containing buffer, MV and chlorinated substrate) were equilibrated overnight. After equilibration, the reductant Ti(III) citrate (pH 7) was added to each vial to a final concentration of 5 mM. This was added directly before the assays to prevent pre-mature oxidation of the reductant and any unintended reactions with the substrates. Further details of the reaction vial setup—including exact concentrations of substrate used—and the assay procedure can be found in Supplemental Text S2.

Trichloroethene (TCE) was tested as an inhibitor for CF dechlorination. Glass bottles (255 mL) with mininert caps were set up with 60 mL of the buffer (50 mM Tris-HCl [pH 7.5] and 1 mM

MV). TCE was delivered to a concentration of 50 μM using a TCE-saturated water stock. The stock solution was equilibrated overnight and then aliquoted to the 11-mL reaction mixture vials to all have the same amount of TCE. The substrate, CF, and Ti(III) citrate were delivered into the vials as previously stated.

Kinetic Assay – Reaction

Purified RDases were thawed on ice and diluted in 50 mM Tris-HCl (pH 7.5) to an RDase concentration of 100 nM. Four—one for each enzyme and an enzyme-free control—1-mL glass, gas-tight Hamilton syringes with a 3.2 mm diameter stainless steel washer inside the barrel of the syringe were used to perform the reactions. The reactions were performed by taking up 900 μL of the assay buffer from the prepared reaction mixture vial and then 100 μL of the diluted enzyme, or buffer for the enzyme-free controls. The reaction was agitated by continually inverting the syringe and letting the washer move through the barrel to physically mix the solution. The reactions were run for 2 min in the case of the CF and 1,1,1-TCA assays, and 5 min for the 1,1,2-TCA assays. At the end of the incubation, the 1-mL reaction was injected via a submerged needle into 5 mL HCl acidified water (pH <2) in an 11-mL GC headspace autosampler vial and immediately sealed by crimping with a Teflon-coated septum. The assays were always carried out in order of the lowest substrate concentration to the highest concentration. The same syringe was used for each enzyme or control and washed between reactions with 1 mL of anaerobic acidified water and 1 mL of anaerobic double-deionized water. A schematic of the reaction procedure is in Figure S2.

While the reactions were performed at room temperature, the exact temperature could not be controlled in the glovebox. A thermometer was placed in the glovebox, and the temperature at the time of each assay was recorded. Temperatures varied between 20–25°C, a comparison of rate as a function of temperature using CF as a substrate is in Supplemental Text S5.

The 1,1,1-TCA kinetic curve was constructed using two sets of data and outliers were identified and removed from the dataset. Outliers occurred when 1,1,1-TCA was delivered using a larger volume (>250 μL) of saturated stock of 1,1,1-TCA was supplied. The outliers were identified visually by the oxidation of methyl viologen, i.e. the depletion of the electron donor, and were confirmed by 1,1-dichloroethene (DCE) in the negative controls. This is because 1,1,1-TCA is unstable in water and can undergo β-elimination to form 1,1-DCE and hydrolysis to form acetic acid [24,25]. The electron donor was often consumed by acetic acid present in the saturated water

stock, causing the catalysis to be limited by electron supply and underestimating the enzyme rate. Increasing the number of reactions performed for 1,1,1-TCA gave more confidence in the model fit despite the uneven coverage along the Michaelis-Menten curve due to interference by the hydrolysis products.

All raw data (including outliers) for each kinetic trial is available in Table S4. Negative control data and raw product masses for each reaction are in Supplemental Text S6.

Analytical Procedures (Gas Chromatography)

GC analysis was carried out on an Agilent 7890A GC instrument with FID equipped with an Agilent G1888 headspace autosampler. All samples were measured with the same instrument method using an Agilent GS-Q plot column (30 m length, 0.53 mm diameter). Helium was used as the carrier gas with a flow rate of 11 mL/min. The 11-mL headspace autosampler vials containing acidified samples were loaded on the autosampler tray, where they were first equilibrated to 70°C for 40 min, then 3 mL of headspace was sampled via a heated transfer line and injected onto the column by a packed inlet maintained at 200°C. After injection, the oven was held at 35°C for 1.5 min then the temperature was ramped up 15°C/min until 100°C was reached. The ramp rate was then reduced to 5°C/min until 185°C was reached where the temperature was held for 10 min. Finally, the column was cleared by ramping the temp 20°C/min to 200°C and holding for 10 min. The FID detector was set to 250°C and data were collected and analyzed using Agilent ChemStation Rev. B.04.02 SP1 software.

External calibration curves were used for each substrate and product to translate the chromatogram peak area to liquid concentration and total nmol per reaction volume. Standard mixes containing all substrates and products of interest were made in sealed methanolic stocks to prevent partitioning into headspace. Standards are prepared by measuring the desired amount of methanolic stock into HCl acidified water to a final volume of 6 mL in the 11-mL headspace vials and immediately crimped. Standard curves were run using five known liquid concentration levels of the standard mix, each run in triplicate. The response factor for each compound, derived from the standard curve, was used to convert peak areas to liquid concentrations. One standard was run with each GC-FID batch to ensure consistent calibration.

Data Processing

The sum of the remaining substrate and products was used to determine the initial substrate concentration in each reaction. The rate was determined by dividing the amount of product (nmol or mg) by the assay time (s) and the mass of RDase in the assay (mg). Error in the protein concentration and an estimated variance of 2-3 s for the incubation time were used as uncertainty in the rate values.

Kinetic Model Fitting

The kinetic data were plotted in Python3 and fit with various Michaelis-Menten kinetic models with and without inhibition using the LMFIT package [26]. The equations of the models tested and their assessment are described in Supplemental Texts S3 and S4. Models were produced using the least squares method and included experimental error in the residual calculation. Data for CF, 1,1,1-TCA, and 1,1,2-TCA without external inhibitors were fit to a typical Michaelis-Menten kinetic expression with and without a term for substrate inhibition. The presence of substrate inhibition was determined by the model of best fit. The best-fit model was selected based on reducing the R^2, Akaike Information Criterion, and the standard deviation of the residuals. The kinetic parameters V_{max} (nmol/s/mg), K_M (μM), and $K_{I,sub}$ (μM; if applicable) were extracted from the models. The k_{cat} (s^{-1}) was calculated by multiplying the V_{max} by the mass of the protein (48 kDa; 48 000 g/mol) to convert the protein mass from mg to nmol. All calculated kinetic parameters—in μM and mg/L units—and fit evaluations can be found in Tables S5-S7.

To determine the inhibition constant, $K_{I,inh}$, of TCE for each enzyme, first, the V_{max}, K_M, and $K_{I,sub}$ (if applicable) values were determined by the uninhibited CF assay performed on the same day. These values were then set as constants and the TCE-inhibited kinetic data was fit with models for competitive, non-competitive, and uncompetitive inhibition. The best-fit model was selected based on reducing the R^2, Akaike Information Criterion, and the standard deviation of the residuals. The calculated kinetic parameters and fit evaluation can be found in Table S8.

Kinetic analysis of 1,1,2-TCA was performed differently than the other substrates because two different products are formed (scheme in Figure S3B). The K_M and $K_{I,sub}$ were calculated by modelling the overall 1,1,2-TCA consumption. The reaction rates for each product were then determined by modelling the production rates with the K_M and $K_{I,sub}$ set as the values determined

from the overall rate. A detailed discussion about the 1,1,2-TCA kinetic analysis can be found in Supplemental Text S3.

Protein Models

Protein models of TmrA and CfrA were retrieved from AlphaFill [27]. AlphaFill contains a database of AlphaFold2 models of all sequences available in UniProt and docks cofactors into the models based on homology to known crystal structures [27,28]. Structures for TmrA and CfrA with cobalamin and two [4Fe-4S] clusters were extracted and further relaxed using YASARA energy minimization server [29]. The AcdA model was generated directly from AlphaFold2 without the cofactors. The crystal structure of PceA (PBD ID: 4ur0) was used as a comparison of the conserved active site residues [10]. All structures were visualized and analyzed, and figures were generated using PyMOL Molecular Graphics System v2.3.4 [30].

Results & Discussion

Kinetic Assay Set-Up

While the activity of several chloroalkane RDases has been studied using cell-free lysates from mixed cultures, direct comparisons of these enzymes are limited. Using a heterologous expression system in *E. coli*, we have produced known CF-reductases: CfrA from *Dehalobacter* sp. CF, TmrA from *Dehalobacter* sp. UNSWDHB, and AcdA from the SC05-UT enrichment culture [16,17,31]. Previous reports of TmrA, CfrA, and AcdA activity show very similar profiles with activity on CF, 1,1,1-TCA, and 1,1,2-TCA; TmrA and AcdA also have activity on 1,1-dichloroethane (DCA), while CfrA does not [14,16,17,20,32]. Yet the enzymes have distinct isotope fractionation for chlorine and carbon when using CF as a substrate [18,19]. Contrasting fractionation patterns can indirectly inform about differences in the rate-determining step of catalysis thus these enzymes are predicted to have varied interactions with CF [18,19]. This kinetic comparison will further support the disparity in the catalytic activity of these highly similar enzymes.

Kinetic assays were conducted assuming that the chlorinated solvent is the only limiting substrate; using excess Ti(III) citrate as the electron donor and short incubation times (2-5 mins) to capture the initial rates. RDases are dependent on an external supply of electrons for catalysis, and thus, if the electron donor were limiting (i.e. if it were not in excess of the target substrate),

then the apparent rate for each substrate would not be truly representative of the enzymes' capabilities. This limitation could be a factor in previous studies that generally incubated the cell-free lysate reactions for 1-2 hours using 2 mM Ti(III) citrate [14,31,33–35]. Overall, the rates observed in this study are much greater than those observed in the literature due to the inability to accurately quantify the RDase in the cell-free lysate and longer incubation times.

It is important to note that in the native OHRB, the rate-limiting step of respiration may be the supply of electrons through the electron transport chain rather than the RDase activity, as suggested previously [33,36]. This would reduce the organism's observed rate of reductive dehalogenation. Our study focuses solely on the rate dictated by the dehalogenation of the supplied organohalide substrate. Additionally, due to the fluctuation of the room temperature (discussed further in Supplemental Text S5), we will only compare assays performed at the same temperature.

Activity on Chloroform and 1,1,1-Trichloroethane (Methyl Chloroform)

Despite CF and 1,1,1-TCA differing by only one methyl group, RDase activity varies significantly between these compounds. Figure 1A and Table 1 show that TmrA has the highest V_{max} for CF (1100 ± 160 nmol/s/mg) compared to CfrA (580 ± 40 nmol/s/mg) and AcdA (710 ± 120 nmol/s/mg). Conversely, with 1,1,1-TCA as a substrate, CfrA has a V_{max} (520 ± 100 nmol/s/mg) roughly double that of TmrA and AcdA, even at low substrate concentrations (Figure 1B/D).

At high concentrations of CF, TmrA ($K_{I,CF}$ = 2600 ± 1900 μM) and AcdA ($K_{I,CF}$ = 610 ± 240 μM) experience substrate inhibition, but CfrA does not. Substrate inhibition occurs when the substrate binds unproductively and prevents catalysis, thereby reducing enzyme activity as substrate concentration increases. A low $K_{I,sub}$ corresponds to stronger inhibition because the value represents the concentration needed to reduce the enzyme to half of its maximum rate. This principle is the same for external inhibitors. With a lower $K_{I,CF}$, AcdA experiences stronger substrate inhibition, but at concentrations of CF sub 100 μM the rate of activity is very similar to TmrA (Figure 1C).

CfrA dechlorinates CF and 1,1,1-TCA as substrates at similar rates (V_{max}), but with a lower K_M of 82 ± 12 μM for CF and versus 180 ± 60 μM for 1,1,1-TCA (Table 1). This trend of affinity aligns with previously published data despite the absolute values being greater [33,35,37]. This

inconsitency in K_M values but agreement in relative trend is also seen with TmrA (Table 1). These discrepancies between previous data could be due to the difference in incubation time and supply of Ti(III) citrate. Another possible cause for a difference in K_M is due to the use of cell-free lysates from the native organism. The catalytic subunit (RdhA) could have protein-protein interactions, such as with the RdhB anchor protein, that result in a change in the interaction between the RdhA and the substrate.

AcdA has the highest affinity for CF with a K_M of 29 ± 8 μM, and a K_M 10-fold larger with 1,1,1-TCA (Table 1). Both AcdA and TmrA have much higher affinities for CF than 1,1,1-TCA suggesting that they have a more compact active site than CfrA, whose difference in K_M is not as drastic.

Another discrepancy between this data and published data for CfrA is the observed inhibition by 1,1,1-TCA. Cell-free extracts containing CfrA were found to experience inhibition by 1,1,1-TCA with a $K_{I,sub}$ range of 300-1000 μM [34,35]. In this work, efforts to fit the 1,1,1-TCA kinetic data with a substrate-inhibition model were unsuccessful, most likely due to the higher variance in reaction rate which resulted from abiotic hydrolysis of 1,1,1-TCA to acetic acid in the substrate stocks. This variance could be due to the presence of hydrolysis product acetic acid in the substrate stock consuming the electron donor or the low solubility of 1,1,1-TCA [24,25]. 1,1,1-TCA has a low solubility (~9 mM) in water [38], and though the tested concentrations are within this threshold, the matrix could interfere with the solubility, causing more variability in the rates. The cell-free extract experiments could have suffered from the same confounding variables or inhibition of 1,1,1-TCA on the other proteins involved in organohalide respiration reducing the electron flow.

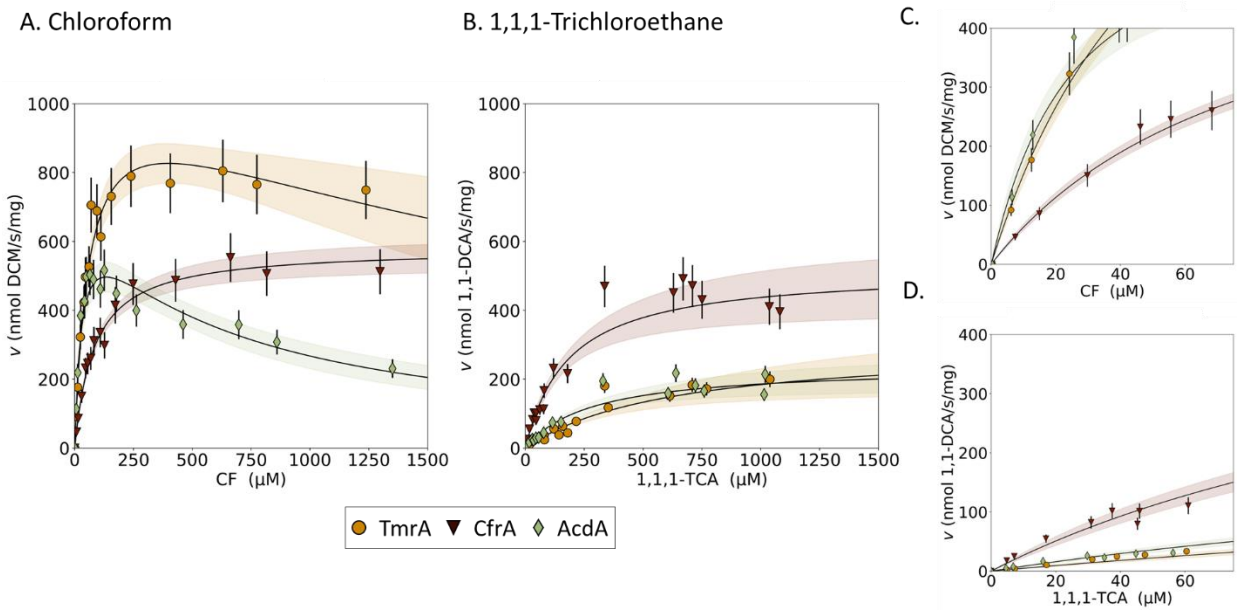

Figure 1. Reaction rate against substrate concentration for TmrA (yellow circles), CfrA (red triangles), and AcdA (green diamonds) using chloroform (CF; A, C) and 1,1,1-trichloroethane (1,1,1-TCA; B, D) as substrates. Plots C and D show the rate of reaction for substrate concentrations lower than 70 μM. Error bars represent the uncertainty in the protein concentration and incubation time propagated in the calculated rate. The black lines are the kinetic models with optimized parameters. The shaded area represents the 95% confidence interval in the predicted model parameters. All reactions were carried out over 2 min at 24°C.

Table 1. Kinetic parameters for CfrA, TmrA, and AcdA using chloroform and 1,1,1-trichloroethane as substrates. All reactions were carried out over 2 min at 24°C. Error is the 95% confidence interval of the values generated by the model.

	Chloroform				**1,1,1-Trichloroethane**			
	K_M (μM)	V_{max} (nmol/s/mg)	k_{cat} (s^{-1})	$K_{I,CF}$ (μM)	K_M μM	V_{max} nmol/s/mg	k_{cat} (s^{-1})	**Reference**
CfrA	82 ± 12	580 ± 40	28 ± 2	n.o.	180 ± 60	520 ± 100	25 ± 5	This study
	n.t.	n.t.		n.t.	45 ± 18 *	1.78 ± 0.65 *		Grostern, 2009 [34]
	22 ± 2.4 *	0.32 ± 0.01 *		n.o.	42 ± 6 *	1.7 ± 0.1 *		Wei, 2016 [33]
	28 ± 4 *	1.3 ± 0.1 *		n.o.	34 ± 27 *	1.8 ± 0.9 *		Grostern, 2010 [35]
TmrA	61 ± 14	1100 ± 160	53 ± 8	2600 ± 1900	630 ± 340	300 ± 130	14 ± 6	This study
	154 ± 41	21 ± 2	1.0 ± 0.1	354	n.t.	n.t.		Jugder, 2017 [14]
	30 ± 12 *	2.7 ± 0.2 *		n.o.	237 ± 53 *	0.55 ± 0.05 *		Wong, 2016 [31]
AcdA	29 ± 8	710 ± 120	34 ± 6	610 ± 240	280 ± 100	240 ± 50	12 ± 2	This study

* measured from cell-free extracts, n.a. = not observed, n.t. = not tested

Trends of Activity on Native Substrates and Correlation with Kinetic Isotope Effects

The kinetic activity trends for CF and 1,1,1-TCA correlate with the substrate structure and enzyme origin. All the RDases have higher V_{max} and lower K_M values with CF, likely because its smaller structure more easily enters and fits in the active site, which could, in turn, enable faster reaction rates. Both TmrA and AcdA originated from CF-contaminated sites: TmrA was identified from *Dehalobacter* sp. UNSWDHB, enriched from a site near Botany Bay in Sydney, Australia that was contaminated with various organochlorines, including CF [6]. AcdA from a CF and DCM degrading culture, SC05, that was enriched from a CF-contaminated site in California, USA [7,8,17]. Whereas CfrA originates from the culture ACT-3 taken from a 1,1,1-TCA and TCE contaminated site in the northeastern USA and enriched on 1,1,1-TCA [5]. As CfrA is the only RDase of the three that had been exposed to and acclimated to 1,1,1-TCA, it has predictably established higher activity on this substrate than the other two. It is quite intriguing that these enzymes from three different parts of the world maintain high sequence similarity but show nuanced differences in their catalytic function.

We can also compare how these kinetic trends compare to the trends in isotope effects. The enrichment factor (ε) is a value that arises from the phenomenon in which substrates that only have light isotopes (C^{12}/Cl^{35}) in the reactive bonds (i.e. the bonds that are breaking or forming) will react faster over those that contain heavy isotopes (C^{13}/Cl^{37}) leading to an enrichment in heavy isotopes in the initial substrate pool [39]. Table 2 shows values of ε—the enrichment of the heavy isotope produces more negative ε, an inverse isotope effect is when the light isotope is enriched and ε is positive [18]. Differences in isotope fractionation can occur due to mechanistic differences in the catalytic slow-step or from "masking effects", which are non-transformation and non-fractioning slow steps that cause suppression of the isotope fractionation. Commitment to catalysis is one such effect, in which a high commitment describes the binding and conversion of a substrate occurring much faster than the reverse dissociation of the substrate and there is less discrimination between heavy and light isotopes (more thorough explanation here [18,39,40]).

The variance in ε values observed for CfrA, TmrA, and AcdA may result from different transformation mechanisms, substrate binding, or structural changes affecting the rate-limiting

step [19]. Although we cannot determine mechanisms from this kinetic analysis, we can compare catalytic efficiency (k_{cat}/K_M). The k_{cat}/K_M takes into account the maximum rate and the binding affinity of the enzymes. Generally, the k_{cat}/K_M increases in the same order that the $\varepsilon^{13}C$ decreases (Table 2). CfrA has similar fractionation values to the abiotic cobalamin reaction, but TmrA and AcdA have high suppression [18,19]. This suppression could be caused by a higher commitment to catalysis given that they have higher k_{cat}/K_M values than CfrA. This trend is less clear in the $\varepsilon^{37}Cl$ values due TmrA's inverse fractionation. Structural diversity between the RDases has been thought to cause these fractionation differences and would also impact their catalytic efficiency [19].

Table 2. The most recently published carbon and chlorine fractionation values for chloroform compared to the kinetic parameters measured in this study. Biotic fractionation values are from respiring cells. Brackets indicate the culture used in the experiments. Error is the 95% confidence interval of the values generated by the model.

Catalyst	$\varepsilon^{13}C$	$\varepsilon^{37}Cl$	k_{cat} (s^{-1})	K_M (μM)	k_{cat}/K_M (s^{-1} μM^{-1})	Reference for epsilon
Abiotic CNCbl	-26.04 ± 0.91‰	-4.00 ± 0.2‰				Heckel, 2019[18]
CfrA (ACT-3)	-26.8 ± 3.2‰	-6.86 ± 0.35‰	28 ± 2	82 ± 12	0.34 ± 0.06	Phillips, 2022[19]
TmrA (CFH2)	-3.1 ± 0.5‰	2.5 ± 0.3‰	53 ± 8	61 ± 14	0.87 ± 0.24	Heckel, 2019[18]
AcdA (SC05)	-1.52 ± 0.34‰	-1.84 ± 0.19v	34 ± 6	29 ± 8	1.2 ± 0.4	Phillips, 2022[19]

CNCbl = cyanocobalamin

Inhibition by Trichloroethene

The inhibition of chloroethenes on chloroalkane reductive dechlorination and vice versa is well established both on the organism and enzyme level [34,41,42]. At mixed-contaminated sites, this inhibition can be unavoidable, but the varying levels of inhibition between enzymes could make specific organisms more suitable for such locations. We assessed the inhibition of CF-dechlorination by TCE; a known inhibitor of CfrA [33,34]. While this is not an exhaustive assessment of inhibition, it provides some perspective on the differences in sensitivity between the three RDases to external inhibition.

The enzyme kinetics on CF were compared with no TCE and with ~45 μM TCE in the assay mixture. The $K_{I,TCE}$ of TCE was calculated using the same V_{max}, K_M, and $K_{I,CF}$ (TmrA and AcdA only) calculated from the uninhibited data taken on the same day. All enzymes were fit with

competitive, uncompetitive, and non-competitive inhibition models and the best-fit model was chosen as the mode of inhibition.

TmrA and AcdA had the best fit with uncompetitive type inhibition, whereas CfrA had the best fit with non-competitive inhibition (Table S8). However, in the *Organohalide-Respiring Bacteria* textbook, Wei *et al*. performed a full inhibition series to determine that CfrA demonstrated uncompetitive inhibition by TCE [33]. In accordance, the data presented here is calculated from the uncompetitive inhibition model for CfrA, which still produced a good fit. All three enzymes experienced some level of inhibition by TCE (Figure 2). AcdA had the most drastic decrease in apparent activity, with a $K_{I,TCE}$ of 16 ± 1 μM (Table 3). CfrA and TmrA have similar $K_{I,TCE}$ values of 85 ± 24 μM and 92 ± 20 μM, respectively. While the inhibition by TCE is expected, it is curious that AcdA is more inhibited by TCE than TmrA and CfrA.

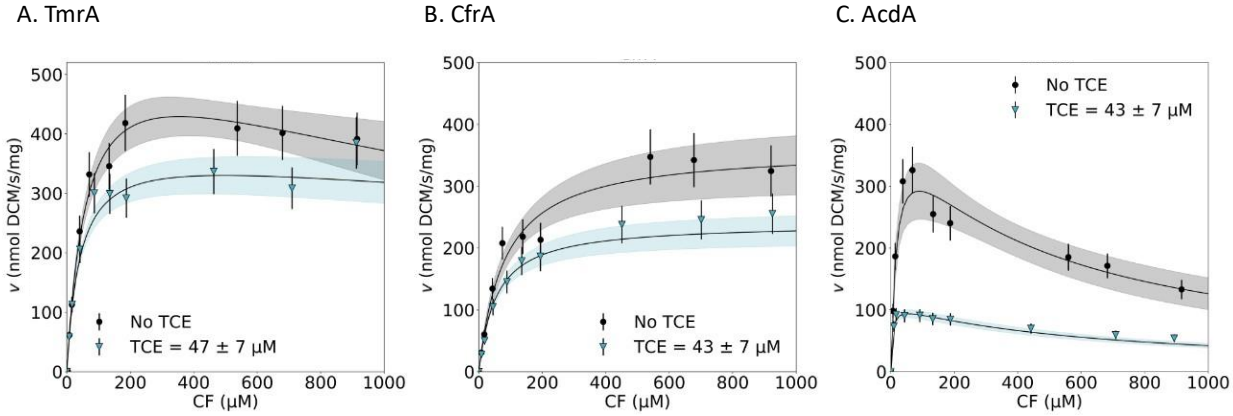

Figure 2. Reaction rate against substrate concentration for TmrA (A), CfrA (B), and AcdA (B) using chloroform (CF) as a substrate either with trichloroethane (TCE) inhibition (blue triangle) or without (black circle). The average concentration of TCE between all reactions is presented on each plot, the error represents the standard deviation. Error bars represent the uncertainty in the protein concentration and incubation time propagated in the calculated rate. The black lines show the optimized kinetic model. The shaded area represents the 95% confidence interval in the predicted model parameters. All reactions were carried out over 2 min at 20°C.

Table 3. Inhibition constant (K_I) of trichloroethane measured for CfrA, TmrA, and AcdA using chloroform as a substrate. All reactions were carried out over 2 min at 20°C. Error is the 95% confidence interval of the values generated by the model.

	$K_{I,TCE}$ (µM)	Reference
CfrA	85 ± 24	This study
	40 ± 3.1 *	(Wei, 2016) [33]
TmrA	92 ± 20	This study
AcdA	16 ± 1	This study

* measured from cell-free extracts

Kinetics on 1,1,2-Trichloroethane

Another stark difference between TmrA, CfrA, and AcdA is their transformation of 1,1,2-TCA. 1,1,2-TCA is a peculiar substrate for RDases because it can undergo both the typical hydrogenolysis to form 1,2-DCA or dihaloelimination to form vinyl chloride (VC). The dihaloelimination of 1,1,2-TCA is strongly favoured as it has a much higher redox potential (E_0' = 1063 mV, H_2 as donor) than the hydrogenolysis reaction (862 mV) [43]. Dihaloelimination can occur abiotically by reduced cobalamin at room temperature and neutral pH [20], it has also been observed by many RDases of varying specificities and most likely occurs easily once the substrate enters the active site [20,44]. Enzymes in OG 97 are known to catalyze both reactions, but the product of 1,1,2-TCA dechlorination can be very consequential as VC is of higher regulatory concern and a known inhibitor of the dechlorination of co-contaminants CF and 1,1,1-TCA [33,3420,31,45,46].

TmrA has the greatest overall turnover of 1,1,2-TCA, with over double the V_{max} of CfrA and AcdA (Figure 3A, Table 4). Each enzyme experiences substrate inhibition to varying degrees, but all with relatively high $K_{I,TCA}$ values over 2 mM (270 mg/L). The enzymes also have a wide range in K_M values, with AcdA having the strongest affinity and CfrA having the weakest with a K_M almost 10-fold higher than AcdA. This means that at lower concentrations, which are likely to be seen at contamination sites, CfrA will work at a much lower rate than AcdA or TmrA. Again, TmrA has a higher K_M than what was reported in the literature, perhaps there is some component of the cell-free extract that limits the activity on this substrate or changes the interaction with TmrA [31].

452 Regardless of overall activity, in the transformation of 1,1,2-TCA, it is important to look
453 at the production of the two substrates 1,2-DCA and VC separately. All three enzymes perform
454 hydrogenolysis to 1,2-DCA, but TmrA still has the fastest V_{max} (Figure 3C, Table 4). TmrA and
455 AcdA both perform the dihaloelimination reaction to form VC with comparable V_{max} values
456 (TmrA, 490 ± 20 nmol/s/mg; AcdA, 480 ± 15 nmol/s/mg). However, AcdA has a slightly higher
457 rate of reaction performing the dihaloelimination than the hydrogenolysis, leading to the major
458 product being VC. Unlike TmrA and AcdA, CfrA produces negligible amounts of VC. This fairly
459 homogeneous production of 1,2-DCA is highly beneficial for treating 1,1,2-TCA contaminated
460 sites to simplify subsequent remediation steps and prevent inhibition by the products on the OHRB
461 processes. Therefore, despite having the slowest rate at field-relevant concentrations, CfrA has the
462 most desirable activity on 1,1,2-TCA.

463 Interestingly, the 1,2-DCA:VC product ratio remains very consistent for each enzyme
464 across increasing 1,1,2-TCA concentrations and incubation times (Figure 3B). A small exception
465 is by CfrA; the initial 99:1 ratio decreases as the substrate concentration increases. However, the
466 absolute production of VC is so small that the percentage of 1,2-DCA is very consistent at 98.7 ±
467 0.6% (Table 4). In the cell-free lysate assays, TmrA produced 77.6 ± 2.9% 1,2-DCA and CfrA
468 produced 98.8 ± 0.5% [20]. Separate 1-hr incubations with purified TmrA resulted in 72.7 ± 0.3%
469 and 74.4 ± 0.3% 1,2-DCA, while the purified AcdA only produced 40.2 ± 0.5% [17,20]. The
470 consistency with varying substrate levels and incubation times is quite astonishing and suggests
471 that the 1,2-DCA:VC ratio is inherent to each OG 97 enzyme and may be able to be predicted if
472 we know the structural features that control it. Deciphering the cause of these differences could
473 enable better prediction of the outcomes at mixed contaminated sites treated with these commercial
474 bioaugmentation cultures.

475

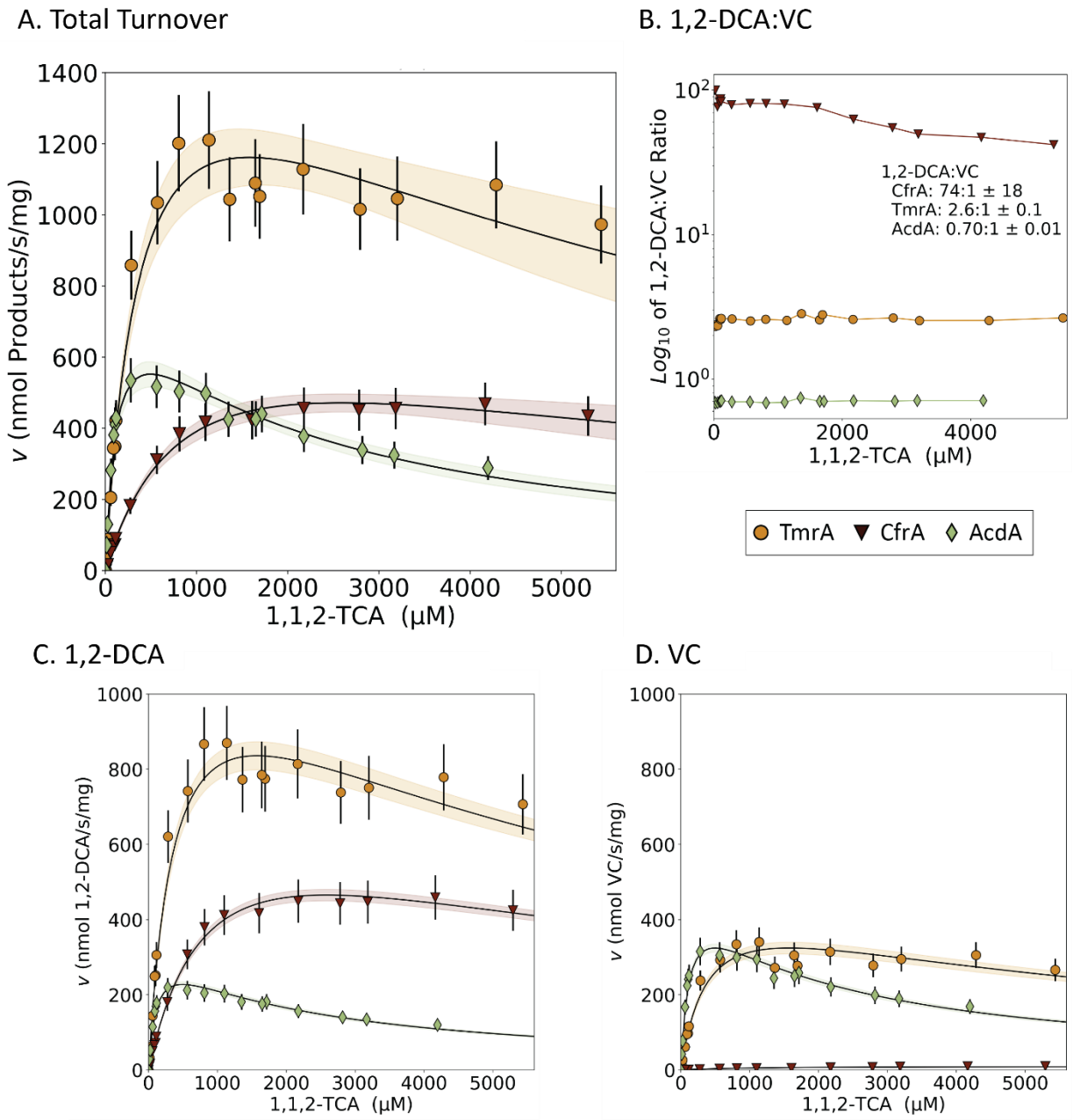

Figure 3. Reaction rate against substrate concentration plots for TmrA (yellow circles), CfrA (red triangles), and AcdA (green diamonds) using 1,1,2-trichloroethane (1,1,2-TCA) as a substrate. (A) is the total turnover of 1,1,2-TCA to all products, (B) is the ratio of 1,2-dichloroethane: vinyl chloride (1,2-DCA:VC) on a $\log_{10}$ scale, (C) shows the rate of 1,2-DCA production and (D) the rate of VC Error bars represent the propagated uncertainty in the protein concentration and incubation time. The black lines show the highest-scoring kinetic model. The coloured area represents the 95% confidence interval in the predicted model parameters. Error for ratio values is the standard deviation between all substrate concentrations. All reactions were carried out over 5 min at 24°C.

Table 4. Kinetic parameters for CfrA, TmrA, and AcdA using 1,1,2-trichloroethane as a substrate resulting in either 1,2-dichloroethane or vinyl chloride as products. All reactions were carried out over 5 min at 24°C. Error is the 95% confidence interval of the values generated by the model.

	K_M (µM)	$K_{I,TCA}$ (µM)	Total V_{max} (nmol/s/mg)	Total k_{cat} (s^{-1})	1,2-DCA V_{max} (nmol/s/mg)	1,2-DCA k_{cat} (s^{-1})	VC V_{max} (nmol/s/mg)	VC k_{cat} (s^{-1})	Percent of 1,2-DCA in product (%)
CfrA	950 ± 220	7100 ± 4400	820 ± 160	39 ± 4	810 ± 20	38 ± 0.5	10 ± 0.6	0.48 ± 0.01	98.7 ± 0.6
TmrA	400 ± 96	6200 ± 3700	1800 ± 320	86 ± 8	1300 ± 50	62 ± 1	490 ± 20	24 ± 0.5	72.0 ± 1.1
	62 ± 19 [a]	n.o.	109 ± 10 [a]		n.d.		n.d.		n.d.
AcdA	120 ± 20	2000 ± 550	820 ± 100	39 ± 2	340 ± 10	16 ± 0.5	480 ± 15	23 ± 0.5	41.2 ± 0.5

[a] values measured from cell-free extracts from Wong, 2016 [31]
n.o. = not observed, n.d. = not determined, TCA = trichloroethane, DCA = dichloroethane, VC = vinyl chloride

Variance in Catalytic Residues

Despite over 95% amino acid sequence identity equating only 15–21 amino acid differences (Supplemental Text S7), CfrA, TmrA, and AcdA exhibit distinct kinetic characteristics. Since these enzymes were all expressed heterologously, these differences must be attributed to the peptide sequence rather than variations within the actual organism—such as the type of cobamide used, which can affect the dechlorination activity [47–49].

Although experimentally derived structures of chloroalkane reductases remain elusive, protein modelling offers insights into potential sources of these mechanistic variations. The resolution of the PceA (*Sulfurospirillum multivorans*) and NpRdhA (*Nitratireductor pacificus* pht-3B) crystal structures revealed several highly conserved active site residues critical for activity [10,11]. Many differences we observe between the OG 97 RDases overlap or collocate with these important residues. The identity of those directly involved in protonation during hydrogenolysis is of particular interest as they directly impact the dehalogenation reaction and, therefore, the rate.

Here, we will reference the PceA structure as it is a respiratory RDase like the OG 97 RDases. PceA features a tyrosine (Tyr246) at the substrate binding site, long thought to be the primary proton donor due to its position and necessity for enzyme activity and conservation in many RDases including those from *Dehalococcoides* and *Dehalobacter* (Supplementary Text S7)

[10,44]. Mutagenic studies also implicated a neighbouring asparagine Asn272 and arginine Arg305 in catalysis [10,11,44], believed to stabilize Tyr246 via H-bonding, evident from their proximity in crystal structures (~3 Å; Figure 4A). However, a recent computational study by Zhang *et al.* suggests that Tyr246 is not likely to be the proton donor because Asn272 and Arg305, both H-bond donors, would stabilize Tyr246 in its deprotonated state [50]. Instead, the more energetically favourable proton donor is Arg305, with Tyr246 and Asn272 positioning Arg305 toward the substrate [50].

The arginine proton donor hypothesis better explains the activity of CfrA and TmrA, which lack tyrosine at this position but have the arginine Arg319 (Figure 4B/C). TmrA instead has a non-H-bonding phenylalanine (Phe260) and CfrA has a cysteine (Cys260), which may have a weaker H-bond due to the distance (3.3 Å in the model) and leaves a larger space in the active site. Both enzymes have serine (Ser286) instead of Asn272, capable of H-bonding. In CfrA, the distance between Ser286 and Cys260 (~6.5 Å) likely prevents interaction; TmrA lacks a nearby H-bond acceptor.

AcdA retains the conserved tyrosine (Tyr260) and arginine (Arg319) but has alanine (Ala286) instead of asparagine (Figure 4D). This asparagine is less conserved in RDases (Supplemental Text S7), so its exact role is unclear, but a network of interactions could potentially affect the catalytic residue positioning relative to substrates.

Despite their high sequence identity, TmrA, CfrA, and AcdA have drastic differences in these ostensibly highly conserved residues that likely influence their kinetic properties. Phillips *et al.* also identified other residues (Tyr80, Leu388, and Met391 in CfrA; Phe80, Phe388, and Trp391 in TmrA and AcdA) as possible sources of isotopic fractionation variance. Future mutant studies should explore these catalysis-implicated residues to understand their impact on kinetic characteristics and isotope effects.

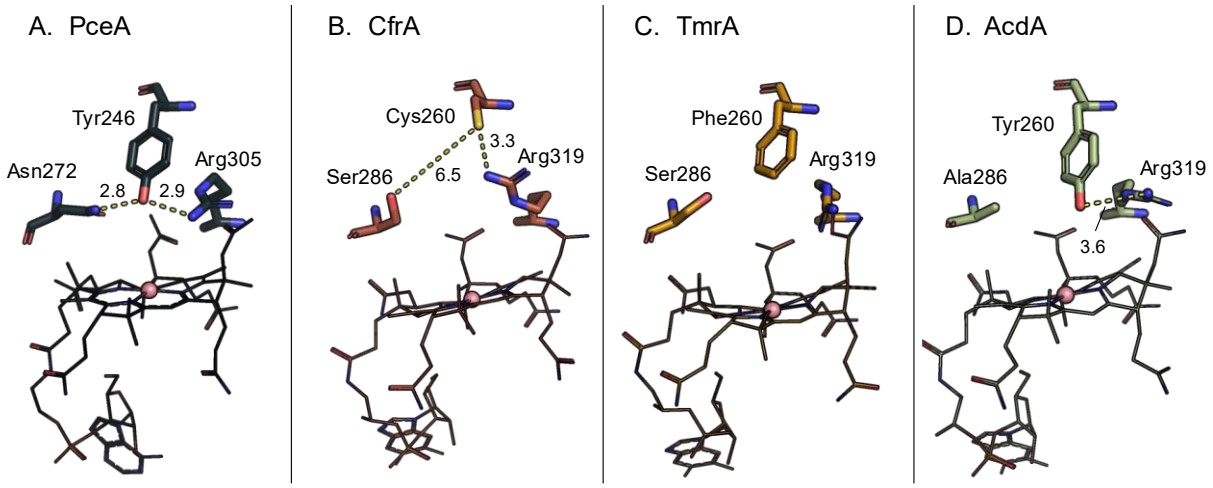

Figure 4. The conserved active site residues in the PceA crystal structure with predicted catalytic activity and the corresponding residues in CfrA, TmrA, and AcdA protein models. Distances between key residues are shown as dashed lines with the distance in angstroms. PDB ID: 4ur0 [10].

Implications for Bioremediation

Kinetic characteristics of RDases can be an important indicator for behaviour in a mixed-contaminant site and provide an estimation for the rate that degradation is expected to be observed. At a contaminated site, the difference in activity can be pronounced when external inhibitors are present, as was evident with the varying levels of inhibition by TCE on each enzyme. In a scenario where CF and TCE are present at a site, the typical strategy involves reducing the CF concentration to avoid inhibiting TCE-dechlorinating organisms. However, the efficiency of the AcdA-containing culture, SC05, will be greatly affected by the presence of TCE, making the augmentation cultures producing CfrA or TmrA more suitable for the task. Additionally, the substrate inhibition observed could impact the maintenance of the mixed cultures that these enzymes originate from. For example, the SC05 culture that AcdA originates is typically maintained with CF concentrations over its $K_{I,sub}$ (610 μM) [7,8]. This means that the SC05 *Dehalobacter* is most likely not growing at its highest rate since AcdA is inhibited by the high CF concentrations and only performs at a fraction of its maximum rate.

Establishing enzymatic rates can also be useful for monitoring both natural attenuation and bioaugmentation efforts. Recent reports have combined quantitative PCR with quantitative proteomics to measure the presence of RDases in aquifers and used published kinetic coefficients

to successfully determine the rate at which target contaminant degradation will occur by natural attenuation [51,52]. Increasing the library of RDase kinetic coefficients will facilitate the implementation of this technique in a variety of cases, and elucidating nuances between similar enzymes will increase the accuracy of these conclusions.

In this work, we have compared the kinetic characteristics of three similar *Dehalobacter* chloroalkane-reductases—TmrA, CfrA, and AcdA—and found considerable differences in their maximum rates, inhibition by their substrates, inhibition by TCE, and in the manner that they dechlorinate 1,1,2-TCA. This is the first comparative kinetic study of highly similar RDases and demonstrates that despite having near-identical protein sequences, RDases can exhibit distinct behaviour. Moreover, this comparison underscores the suitability of certain RDases for particular conditions. Investigating the structural features responsible for these variances will elucidate the significance of key active site residues and facilitate future engineering of more efficient RDases.

Acknowledgements

This study was supported by an Ontario Graduate Scholarship to K.J.P and a Canadian Research Chair to E.A.E. The funders had no role in study design, data collection and interpretation, or the decision to submit the work for publication.

E.A.E. and K.J.P. conceived of the experiments, all experiments were conducted by K.J.P. K.J.P. and E.A.E. drafted the manuscript. We thank Olivia Bulka for the sequence of AcdA and Miya Tseng-West for assistance in its cloning. We thank the Booker Lab from Pennsylvania State University for gifting the *pBAD42-BtuCEDFB* plasmid, and the Antony Lab from the St. Louis University School of Medicine and Kiley lab from the University of Wisconsin-Madison for gifting us the *E. coli* BL21(DE3) *cat-araC*-P_{BAD}-*suf*, *ΔiscR::kan*, *ΔhimA*::Tet^R.

References

(1) Agency for Toxic Substances and Disease Registry (ATSDR). ATSDR's Substance Priority List https://www.atsdr.cdc.gov/spl/index.html.

(2) Agency for Toxic Substances and Disease Registry (ATSDR). *Toxicological Profile for 1,1,2-Trichloroethane*; 2021. https://doi.org/http://dx.doi.org/10.1155/2013/286524.

(3) Agency for Toxic Substances and Disease Registry (ATSDR). *Toxicological Profile for 1,1,1-Trichloroethane (Draft for Public Comment)*; 2023. https://doi.org/http://dx.doi.org/10.1155/2013/286524.

(4) Agency for Toxic Substances and Disease Registry (ATSDR). *Toxicological Profile for Chloroform (Draft for Public Comment)*; 2024. https://doi.org/10.1201/9781420061888_ch59.

(5) Grostern, A.; Edwards, E. A. A 1,1,1-Trichloroethane-Degrading Anaerobic Mixed Microbial Culture Enhances Biotransformation of Mixtures of Chlorinated Ethenes and Ethanes. *Appl. Environ. Microbiol.* **2006**, *72* (12), 7849–7856. https://doi.org/10.1128/AEM.01269-06.

(6) Lee, M.; Low, A.; Zemb, O.; Koenig, J.; Michaelsen, A.; Manefield, M. Complete Chloroform Dechlorination by Organochlorine Respiration and Fermentation. *Environ. Microbiol.* **2012**, *14*, 883–894. https://doi.org/10.1111/j.1462-2920.2011.02656.x.

(7) Wang, H.; Yu, R.; Webb, J.; Dollar, P.; Freedman, D. L. Anaerobic Biodegradation of Chloroform and Dichloromethane with a *Dehalobacter* Enrichment Culture. *Appl. Environ. Microbiol.* **2022**, *88* (4), e01970-21. https://doi.org/10.1128/aem.01970-21.

(8) Bulka, O.; Webb, J.; Dworatzek, S.; Mahadevan, R.; Edwards, E. A. A Multifunctional *Dehalobacter*? Tandem Chloroform and Dichloromethane Degradation in a Mixed Microbial Culture. *Environ. Sci. Technol.* **2023**, *57* (48), 19912–19920. https://doi.org/10.1021/acs.est.3c06686.

(9) Fincker, M.; Spormann, A. M. Biochemistry of Catabolic Reductive Dehalogenation. *Annu. Rev. Biochem.* **2017**, *86* (1), 357–386. https://doi.org/10.1146/annurev-biochem-061516-044829.

(10) Bommer, M.; Kunze, C.; Fesseler, J.; Schubert, T.; Diekert, G.; Dobbek, H. Structural Basis for Organohalide Respiration. *Science* **2014**, *346* (6208), 455–458.

(11) Payne, K. A. P.; Quezada, C. P.; Fisher, K.; Dunstan, M. S.; Collins, F. A.; Sjuts, H.; Levy, C.; Hay, S.; Rigby, S. E. J.; Leys, D. Reductive Dehalogenase Structure Suggests a Mechanism for B_{12}-Dependent Dehalogenation. *Nature* **2015**, *517*, 513–516. https://doi.org/10.1038/nature13901.

(12) Hug, L. A.; Maphosa, F.; Leys, D.; Löffler, F. E.; Smidt, H.; Edwards, E. A.; Adrian, L. Overview of Organohalide-Respiring Bacteria and a Proposal for a Classification System for Reductive Dehalogenases. *Philos. Trans. R. Soc. B* **2013**, *368*, 20120322.

(13) Molenda, O.; Puentes Jácome, L. A.; Cao, X.; Nesbø, C. L.; Tang, S.; Morson, N.; Patron, J.; Lomheim, L.; Wishart, D. S.; Edwards, E. A. Insights into Origins and Function of the

Unexplored Majority of the Reductive Dehalogenase Gene Family as a Result of Genome Assembly and Ortholog Group Classification. *Environ. Sci. Process. Impacts* **2020**, *22* (3), 663–678. https://doi.org/10.1039/c9em00605b.

(14) Jugder, B. E.; Bohl, S.; Lebhar, H.; Healey, R. D.; Manefield, M.; Marquis, C. P.; Lee, M. A Bacterial Chloroform Reductive Dehalogenase: Purification and Biochemical Characterization. *Microb. Biotechnol.* **2017**, *10* (6), 1640–1648. https://doi.org/10.1111/1751-7915.12745.

(15) Jugder, B.; Ertan, H.; Bohl, S.; Lee, M.; Marquis, C. P.; Manefield, M. Organohalide Respiring Bacteria and Reductive Dehalogenases: Key Tools in Organohalide Bioremediation. *Front. Microbiol.* **2016**, *7* (March), 249. https://doi.org/10.3389/fmicb.2016.00249.

(16) Tang, S.; Edwards, E. A. Identification of *Dehalobacter* Reductive Dehalogenases That Catalyse Dechlorination of Chloroform, 1,1,1- Trichloroethane and 1,1-Dichloroethane. *Philos. Trans. R. Soc. B* **2013**, *368* (1616), 20120318. https://doi.org/10.1098/rstb.2012.0318.

(17) Bulka, O.; Picott, K.; Mahadevan, R.; Edwards, E. A. From *mec* Cassette to *rdhA*: A Key *Dehalobacter* Genomic Neighborhood in a Chloroform and Dichloromethane–Transforming Microbial Consortium. *Appl. Environ. Microbiol.* **2024**, *80*, e00732-24. https://doi.org/https://doi.org/10.1128/aem.00732-24.

(18) Heckel, B.; Phillips, E.; Edwards, E.; Sherwood Lollar, B.; Elsner, M.; Manefield, M. J.; Lee, M. Reductive Dehalogenation of Trichloromethane by Two Different *Dehalobacter restrictus* Strains Reveal Opposing Dual Element Isotope Effects. *Environ. Sci. Technol.* **2019**, *53* (5), 2332–2343. https://doi.org/10.1021/acs.est.8b03717.

(19) Phillips, E.; Bulka, O.; Picott, K.; Kümmel, S.; Edwards, E. A.; Nijenhuis, I.; Gehre, M.; Dworatzek, S.; Webb, J.; Sherwood Lollar, B. Investigation of Active Site Amino Acid Influence on Carbon and Chlorine Isotope Fractionation during Reductive Dechlorination. *FEMS Microbiol. Ecol.* **2022**, *98* (8), fiac072. https://doi.org/10.1093/femsec/fiac072.

(20) Picott, K. J.; Flick, R.; Edwards, E. A. Heterologous Expression of Active *Dehalobacter* Respiratory Reductive Dehalogenases in *Escherichia coli*. *Appl. Environ. Microbiol.* **2022**, *88* (3), e01993-21. https://doi.org/10.1128/AEM.01993-21.

(21) Corless, E. I.; Mettert, E. L.; Kiley, P. J.; Antony, E. Elevated Expression of a Functional Suf Pathway in *Escherichia coli* BL21(DE3) Enhances Recombinant Production of an Iron-Sulfur Cluster-Containing Protein. *J. Bacteriol.* **2020**, *202* (3), e00496-19.

(22) Lanz, N. D.; Blaszczyk, A. J.; McCarthy, E. L.; Wang, B.; Wang, R. X.; Jones, B. S.; Booker, S. J. Enhanced Solubilization of Class B Radical S-Adenosylmethionine Methylases by Improved Cobalamin Uptake in *Escherichia coli*. *Biochemistry* **2018**, *57* (9), 1475–1490. https://doi.org/10.1021/acs.biochem.7b01205.

(23) Bradford, M. M. A Rapid and Sensitive Method for the Quantitation of Microgram Quantities of Protein Utilizing the Principle of Protein-Dye Binding. *Anal. Biochem.* **1976**, *72*, 248–254. https://doi.org/10.1016/j.cj.2017.04.003.

(24) Gerkens, R. R.; Franklin, J. A. The Rate of Degradation of 1,1,1-Trichloroethane in Water by Hydrolysis and Dehydrochlorination. *Chemosphere* **1989**, *19* (12), 1929–1937.

(25) Vogel, T. M.; McCarty, P. L. Abiotic and Biotic Transformations of 1,1,1-Trichloroethane under Methanogenic Conditions. *Environ. Sci. Technol.* **1987**, *21* (12), 1208–1213. https://doi.org/10.1021/es00165a008.

(26) Newville, M.; Stensitzki, T.; Allen, D. B.; Ingargiola, A. LMFIT: Non-Linear Least-Square Minimization and Curve-Fitting for Python. 2014.

(27) Hekkelman, M. L.; de Vries, I.; Joosten, R. P.; Perrakis, A. AlphaFill: Enriching AlphaFold Models with Ligands and Cofactors. *Nat. Methods* **2023**, *20* (2), 205–213. https://doi.org/10.1038/s41592-022-01685-y.

(28) Jumper, J.; Evans, R.; Pritzel, A.; Green, T.; Figurnov, M.; Ronneberger, O.; Tunyasuvunakool, K.; Bates, R.; Žídek, A.; Potapenko, A.; et al. Highly Accurate Protein Structure Prediction with AlphaFold. *Nature* **2021**, *596*, 583–589. https://doi.org/10.1038/s41586-021-03819-2.

(29) Krieger, E.; Joo, K.; Lee, J.; Lee, J.; Raman, S.; Thompson, J.; Tyka, M.; Baker, D.; Karplus, K. Improving Physical Realism, Stereochemistry, and Side-Chain Accuracy in Homology Modeling: Four Approaches That Performed Well in CASP8. *Proteins Struct. Funct. Bioinforma.* **2009**, *77* (SUPPL. 9), 114–122. https://doi.org/10.1002/prot.22570.

(30) Schrödinger LLC. The PyMOL Molecular Graphics System, Version 2.0.

(31) Wong, Y. K.; Holland, S. I.; Ertan, H.; Manefield, M.; Lee, M. Isolation and Characterization of *Dehalobacter* sp. strain UNSWDHB Capable of Chloroform and Chlorinated Ethane Respiration. *Environ. Microbiol.* **2016**, *18*, 3092–3105. https://doi.org/10.1111/1462-2920.13287.

(32) Jugder, B.-E.; Payne, K. A. P.; Fisher, K.; Bohl, S.; Lebhar, H.; Manefield, M.; Lee, M.; Leys, D.; Marquis, C. P. Heterologous Production and Purification of a Functional Chloroform Reductive Dehalogenase. *ACS Chem. Biol.* **2018**, *13*, 548–552. https://doi.org/10.1021/acschembio.7b00846.

(33) Wei, K.; Grostern, A.; Chan, W. W. M.; Richardson, R. E.; Edwards, E. A. Electron Acceptor Interactions Between Organohalide-Respiring Bacteria: Cross-Feeding, Competition, and Inhibition. In *Organohalide-Respiring Bacteria*; Springer-Verlag Berlin Heidelberg, 2016; pp 283–308.

(34) Grostern, A.; Chan, W. W. M.; Edwards, E. A. 1,1,1-Trichloroethane and 1,1-Dichloroethane Reductive Dechlorination Kinetics and Co-Contaminant Effects in a *Dehalobacter*-Containing Mixed Culture. *Environ. Sci. Technol.* **2009**, *43* (17), 6799–6807.

(35) Grostern, A.; Duhamel, M.; Dworatzek, S.; Edwards, E. A. Chloroform Respiration to Dichloromethane by a *Dehalobacter* Population. *Environ. Microbiol.* **2010**, *12* (4), 1053–1060. https://doi.org/10.1111/j.1462-2920.2009.02150.x.

(36) Nijenhuis, I.; Zinder, S. H. Characterization of Hydrogenase and Reductive Dehalogenase Activities of *Dehalococcoides ethenogenes* Strain 195. *Appl. Environ. Microbiol.* **2005**, *71*

(3), 1664–1667. https://doi.org/10.1128/AEM.71.3.1664-1667.2005.

(37) Grostern, A.; Edwards, E. A. Characterization of a Dehalobacter Coculture That Dechlorinates 1,2-Dichloroethane to Ethene and Identification of the Putative Reductive Dehalogenase Gene. *Appl. Environ. Microbiol.* **2009**, *75* (9), 2684–2693. https://doi.org/10.1128/AEM.02037-08.

(38) Mackay, D.; Shiu, W.-Y.; Ma, K.-C.; Lee, S. C. *Handbook of Physical-Chemical Properties and Environmental Fate for Organic Chemicals*, 2nd ed.; CRC Press, 2006.

(39) Elsner, M.; Zwank, L.; Hunkeler, D.; Schwarzenbach, R. P. A New Concept Linking Observable Stable Isotope Fractionation to Transformation Pathways of Organic Pollutants. *Environ. Sci. Technol.* **2005**, *39*, 6896–6916.

(40) Northrop, D. B. The Expression of Isotope Effects on Enzyme-Catalyzed Reactions. *Annu. Rev. Biochem.* **1981**, *50*, 103–131. https://doi.org/10.1146/annurev.bi.50.070181.000535.

(41) Li, H.; He, J.; Jia, W. The Influence of Gut Microbiota on Drug Metabolism and Toxicity. *Expert Opin. Drug Metab. Toxicol.* **2016**, *12*, 31–40. https://doi.org/10.1517/17425255.2016.1121234.The.

(42) Duhamel, M.; Wehr, S. D.; Yu, L.; Rizvi, H.; Seepersad, D.; Dworatzek, S.; Cox, E. E.; Edwards, E. A. Comparison of Anaerobic Dechlorinating Enrichment Cultures Maintained on Tetrachloroethene, Trichloroethene, cis-Dichloroethene and Vinyl Chloride. *Water Res.* **2002**, *36*, 4193–4202.

(43) Dolfing, J. Energetic Considerations in Organohalide Respiration. In *Organohalide-Respiring Bacteria*; Springer, 2016; pp 31–48.

(44) Kunze, C.; Diekert, G.; Schubert, T. Subtle Changes in the Active Site Architecture Untangled Overlapping Substrate Ranges and Mechanistic Differences of Two Reductive Dehalogenases. *FEBS J.* **2017**, *284* (20), 3520–3535. https://doi.org/10.1111/febs.14258.

(45) Soder-Walz, J. M.; Wasmund, K.; Deobald, D.; Vicent, T.; Adrian, L.; Marco-Urrea, E. Respiratory Protein Interactions in *Dehalobacter* sp. strain 8M Revealed through Genomic and Native Proteomic Analyses. *Environ. Microbiol.* **2023**, 1–17. https://doi.org/10.1111/1462-2920.16464.

(46) Zhao, S.; Ding, C.; He, J. Detoxification of 1,1,2-Trichloroethane to Ethene by *Desulfitobacterium* and Identification of Its Functional Reductase Gene. *PLoS One* **2015**, *10* (4), e0119507. https://doi.org/10.1371/journal.pone.0119507.

(47) Wang, P.-H.; Tang, S.; Nemr, K.; Flick, R.; Yan, J.; Mahadevan, R.; Yakunin, A. F.; Löffler, F. E.; Edwards, E. A. Refined Experimental Annotation Reveals Conserved Corrinoid Autotrophy in Chloroform-Respiring *Dehalobacter* Isolates. *ISME J.* **2017**, *11*, 626–640. https://doi.org/10.1038/ismej.2016.158.

(48) Yan, J.; Şimşir, B.; Farmer, A. T.; Bi, M.; Yang, Y.; Campagna, S. R.; Löffler, F. E. The Corrinoid Cofactor of Reductive Dehalogenases Affects Dechlorination Rates and Extents in Organohalide-Respiring *Dehalococcoides mccartyi*. *ISME J.* **2016**, *10* (5), 1092–1101. https://doi.org/10.1038/ismej.2015.197.

(49) Yan, J.; Bi, M.; Bourdon, A. K.; Farmer, A. T.; Wang, P.-H.; Molenda, O.; Quaile, A. T.; Jiang, N.; Yang, Y.; Yin, Y.; et al. Purinyl-Cobamide Is a Native Prosthetic Group of Reductive Dehalogenases. *Nat. Chem. Biol.* **2018**, *14*, 8–14. https://doi.org/10.1038/nchembio.2512.

(50) Zhang, X.; Wang, Z.; Li, Z.; Shaik, S.; Wang, B. [4Fe-4S]-Mediated Proton-Coupled Electron Transfer Enables the Efficient Degradation of Chloroalkenes by Reductive Dehalogenases. *ACS Catal.* **2023**, *13*, 1173–1185. https://doi.org/10.1021/acscatal.2c06306.

(51) Kucharzyk, K. H.; Murdoch, F. K.; Wilson, J.; Michalsen, M.; Frank, E. L.; Murdoch, R. W.; Istok, J. D.; Hatzinger, P. B.; Mullins, L.; Hill, A. Integrated Advanced Molecular Tools Predict in Situ CVOC Degradation Rates: Field Demonstration. *Environ. Sci. Technol.* **2023**, *58*, 557–569. https://doi.org/10.1021/acs.est.3c06231.

(52) Michalsen, M. M.; Kara Murdoch, F.; Löffler, F. E.; Wilson, J.; Hatzinger, P. B.; Istok, J. D.; Mullins, L.; Hill, A.; Murdoch, R. W.; Condee, C.; et al. Quantitative Proteomics and Quantitative PCR as Predictors of *cis*-1,2-Dichlorethene and Vinyl Chloride Reductive Dechlorination Rates in Bioaugmented Aquifer Microcosms. *ACS ES&T Eng.* **2022**, *2*, 43–53. https://doi.org/10.1021/acsestengg.1c00207.
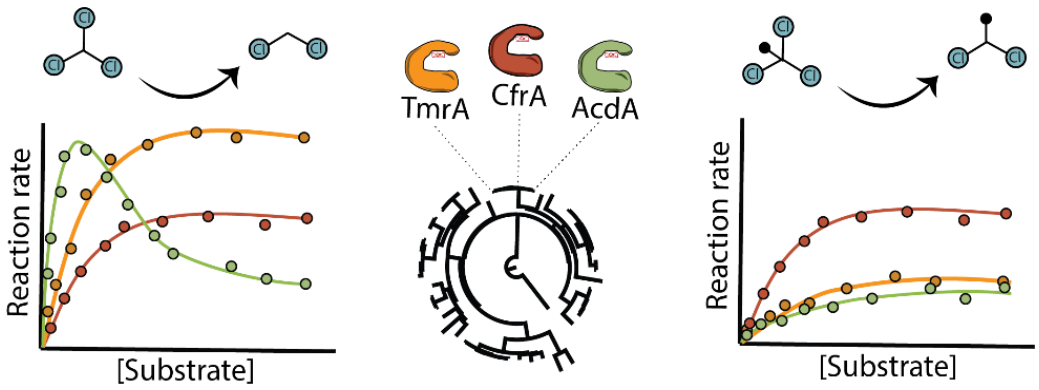
TOC Figure